The effect of coating architecture and defects on the corrosion behaviour of a PVD multilayer Inconel 625/Cr coating

J.L. Daure[1], K.T. Voisey[1], P.H. Shipway[1], D.A. Stewart[2]

Faculty of Engineering, The University of Nottingham, University Park, Nottingham, UK, NG7 2RD.

[2]Rolls- Royce plc, Raynesway, Derby, DE21 7XX

Corresponding author: Katy.Voisey@nottingham.ac.uk

Abstract

This paper investigates the effect of substrate surface finish and deposition conditions of PVD multilayer Inconel 625/Cr coatings on their ability to act as a corrosion-barrier. The corrosion-barrier performance of the coatings was characterized by potentiodynamic testing and salt-spray testing followed by image analysis of the exposed surface; further coating properties were investigated through XRD, SEM, EDX and scratch testing. The results show that multilayering produced the expected improvement in scratch resistance however it did not affect corrosion behaviour. Interrupting the deposition process did not decrease the defect density. Defect density was observed to reduce with decreasing substrate surface finish. The corrosion barrier performance of the multilayer Inconel 625/Cr coating (b_p100 nm) was greatly improved for coatings deposited on a polished substrate. For the multilayer Inconel 625/Cr coating system used in this work multilayering and process interruption did not prevent defects from limiting the corrosion barrier effectiveness of the coatings. Corrosion barrier performance was successfully enhanced by the use of low roughness substrates to minimise the defect density.

Keywords: PVD coatings, growth defects, corrosion, scratch, intermediate treatments, multilayer

1 Introduction

Many coatings which the industrial sector has relied upon for many years are produced by chemical deposition (both electro- and electroless deposition). The production of coatings by this method is coming under increasing pressure due to environmental concerns, with legislation (such as REACH [1]) putting the long term availability of these processes at risk. In particular, physical vapour deposition (PVD) is seen as an attractive coating technique in this regard, as there are few restrictions on the choice of substrate material and the coating process does not cause thermal damage to the substrate. The properties of the coatings can be controlled through the materials and deposition methods used, the coating architecture and the nature of the substrate [2, 3]. PVD coatings are most widely used to enhance wear resistance or surface hardness. While corrosion protection is not usually the main function of these coatings, there is a requirement that they are sufficiently corrosion resistant to survive in their service environment.

The nature of the growth of PVD coatings features numerous nucleation sites which tends to result in a, at least partially, columnar nature of the coatings. The interfaces between adjacent columns can act as pathways for corrosive agents to reach the substrate, thereby preventing the coating from acting as an effective corrosion barrier. The growth of such coatings also closely follows the topography of the substrate surface, and therefore, the substrate surface finish is an important factor in determining the coating properties [4-6]. PVD coatings contain microporosity as well as growth defects, and these growth defects can cause local loss of adhesion and increase the permeability of the coating, therefore reducing the corrosion-barrier performance of the film [5, 7-12].

In order to improve the corrosion barrier properties of PVD coatings, it is important to minimise the density of these defects; many attempts have been made to reduce these defects but they are yet to be eliminated completely [7-10], meaning that such films are not yet generally

competitive with electro- and electroless deposited coatings in terms of corrosion-barrier capabilities. Defects tend to be non-uniformly distributed over the coated surface; the density, shape and size of the defects is dependent on the deposition conditions and the nature of the substrate. Defects can originate from substrate surface irregularities such as pits and asperities, foreign particle contamination on the substrate surface (such as dust and grinding/polishing residues), and from uncontrolled deposition of material from the sputter or evaporation source [8, 10, 12-14]. It is assumed that large defects are related to the cleanliness of the batching room, and it has been shown that some microscopic particles can remain on the substrate surface even after ultrasonic cleaning [9, 12]. During deposition, these particles are coated and create cone like defects (also known as flake defects [8]) which commonly experience high residual stresses, and due to these stresses these cones of coating material may fall off either immediately following deposition or in service, leaving pits in the coating. In addition, some cavities which occur during deposition cannot be completely covered due to the shadowing effect of thin hard coatings [8, 12].

A significant body of research has been reported in the literature describing the effects of the substrate surface finish on the defect density and the mechanical properties of the coatings. It has been demonstrated that a smooth substrate surface finish provides a coating with a lower defect density, and accordingly, not only improves the adhesion of the coating but also improves the corrosion resistance and results in a lower friction coefficient within a tribological couple [6, 14-17]. Panjan et al. have investigated the origin of growth defects and their distribution across a surface, demonstrating that the formation of growth defects is variable, both in time and in space [18].

There are many ways which have been proposed for the improvement in the corrosion-barrier performance of PVD coatings, such as the use of thicker coatings, multilayering, intermediate etching, alloying and through the elimination of droplets by modification of the deposition

process [19-22]. During intermediate etching, the grown film surface is bombarded by ions. This is said to increase growth defect density near the surface in order to create new nucleation sites for the subsequently deposited film, therefore, reducing the density of through-pores and pinholes [19, 23]. Fenker et al. have examined the effect of intermediate etching on the corrosion behaviour of monolithic CrN and multilayer Cr/CrN films as a means of disrupting the film growth (in an attempt to disrupt defect propagation through the film); they found that whilst intermediate etching improves the corrosion resistance of monolithic CrN films, for multilayered coatings the adhesion of the coatings to the substrate was worse after intermediate etching and no improvement could be seen in the corrosion resistance [19].

It has been proposed that the multilayering will serve to block the path of the corrosive agent to the substrate by closing up pores, crevices, defects or failures due to the coatings columnar structure [24-27] (i.e. the multilayering process itself disrupts the growth of the film, including the growth of defects). In terms of tribological properties, multilayers are often used to create a coating which combines a high hardness with a low elastic modulus through alternating of hard and soft layers; the multilayers also improve the resistance of the coating to fracture, due to cracks not being able to propagate from layer to layer. The coating is also able to accommodate substrate deformation (which can occur under load) through shear at the interfaces between individual layers, or by shear within one of the layer types within the multilayer (generally, a material with a low yield strength) [5, 28-30].

This paper seeks to investigate the effects of multilayering, substrate surface finish and coating deposition process conditions on coating defect type and density and to correlate these with the corrosion-barrier behaviour. A multilayer Inconel 625/Cr coating has been selected for the study. The Inconel 625/Cr system was chosen with the intention of generating coatings that were both scratch and corrosion resistant. Both constituents have a desirably good corrosion resistance and the higher strength of the Inconel 625 enables it to act as the harder layer with

Cr acting as the softer layer in order for the multilayer coatings to benefit from the enhanced resistance to fracture by the mechanism described above.

2 Experimental details

2.1 Materials

An M42 high speed steel in the form of Ø30 mm discs, 3 mm thick, with a directional 1200 grit surface finish, HV = 946 ± 12 kg f mm^{-2} was employed as the substrate for scratch tests and a 440C stainless steel (SS) in the form of Ø35 mm discs, 3 mm thick, heat treated to HV = 476 ± 7 kg f mm^{-2}, was employed as the substrate for corrosion tests. Compositions of the substrates, as determined using optical emission spectroscopy on the as ground substrates, are presented in Table 1. Four measurements were taken per substrate and an average was calculated.

The PVD coating materials employed were chromium (Cr) and Inconel 625, the latter being a nickel based superalloy with a composition as shown in table 2 [31]. These materials were deposited either as single layers, or in a multilayer architecture.

2.2 PVD coating

Coatings were deposited at Teer Coatings Ltd. using Closed Field Unbalanced Magnetron Sputter Ion Plating (CFUBMSIP). Two batches of coatings were produced. The initial batch was employed to investigate the effect of the architecture on the scratch and corrosion-barrier performance of multilayer Inconel 625/Cr coatings. In addition to a monolithic Inconel 625 coating, multilayer Inconel 625/Cr coatings with individual layer thicknesses of 10 nm (b_p20 nm), 50 nm (b_p100 nm) and 300 nm (b_p600 nm) were generated (Figure 1). In each case the coating consisted of alternating layers of the two materials, so the repeat distance, or bilayer period, b_p, was twice the layer thickness. For the second batch, the b_p100 nm, multilayer Inconel 625/Cr coating was selected for detailed investigation of the effects of substrate surface

roughness and interrupted deposition conditions on the corrosion-barrier performance of the coatings. This coating system was selected as a balance between the number of multilayer interfaces present in the coating and visibility of distinct layers in SEM micrographs (Figure 1), which allows the effects of any growth defects on coating structure to be readily identified by the disruption of the individual layers. Three different surface finishes were investigated: a unidirectional workshop grind (Ra = 126 ± 8 nm), a unidirectional 1200 grit grind (Ra = 78 ± 12 nm), and a 6μm polish (Ra = 12 ± 4 nm)

Prior to coating, the samples were ultrasonically cleaned in acetone for 15 minutes and then dried before being loaded into the coating system. Once in place, the parts were given a final clean with a methanol-soaked cloth in order to remove any dust. The system was then pumped down for a minimum of an hour to less than 7 x 10^{-5} mbar to remove possible contaminants, before being back filled with argon at 25 sccm.

A pulsed DC argon ion clean of the surface was carried out for 20 minutes in which a negative voltage of 400 V was applied to the samples while a low current of around 0.2 A was applied to the targets with a voltage of around 250 V using a pulsed DC power supply set at a frequency of 250 kHz and pulse width of 500 ns, the deposition pressure used was around 2.6 x 10^{-3} mbar.

In every case, in order to improve the adhesion of the coating to the substrate, the first coating layer deposited was 100 nm of chromium. For multilayer deposition, the Inconel 625 and Cr targets were mounted vertically and opposite each other in the chamber. Substrates were mounted vertically on a cylindrical sample holder that was positioned in the centre of the deposition chamber and which rotated about a vertical axis in the centre of the chamber. When the sample was directly facing the target, the distance between the sample and target was 150 mm. In order to produce distinct multilayers, the rotation speed and deposition rate were selected so that the Cr layers and Inconel 625 layers of the desired thickness were deposited. This cycle of deposition was repeated for the requisite number of rotations to build up the

multilayer coatings. In each case, the process was designed to produce a coating which consisted of Cr layers and Inconel 625 layers of equal thickness. All coatings had a final thickness of ~ 4 μm.

The effect of process continuity was investigated using 440C SS substrates with a 1200 grit surface finish. Two different interrupted process conditions were investigated, namely intermediate etch and interrupted conditions. Both require the coating process to be stopped mid-way. For the intermediate etch process, an ion etch was carried out for 5 minutes on the coating surface during an interruption in the deposition. This process did not require venting of the system, therefore no drop in temperature occurred. For the interrupted conditions, the coating process was stopped mid-way through deposition and the system was vented, in which the temperature dropped to around 50ºC; however, no ion etch was carried out. The system was then pumped down for a minimum of an hour to 7 x 10^{-5} mbar to remove possible contaminants.

2.3 Characterization of coatings

2.3.1 SEM and energy dispersive x-ray (EDX) analysis

Imaging was carried out using two microscopes, a Phillips XL-30 FEG-ESEM and a Zeiss Nvision40 Crossbeam, both using a 20 kV beam. Images of top surfaces and cross-sections were taken using both secondary electron (SE) and back scattered electron (BSE) modes. EDX analysis was performed in the SEM, using spot analysis with counting times of 60 s. Top surface SEM was carried out to determine the number and size of defects in the coatings over a 4300 μm^2 area. Images were taken at 4000x magnification and two images were taken of areas representing the defect density across the whole coating. Defects were categorised by size and shape as linear defects and circular defects. Circular defects were separated into three groups: larger than 3 μm, between 1 and 3 μm and smaller than 1 μm.

2.4 XRD

X-ray diffraction (XRD) was carried out using a Bruker D8 Advance, using monochromatic Cu-Kα radiation with a wavelength (λ) of 1.5418 nm, emitted through a 0.6 mm slit. A glancing angle was used with a 2θ step size of 0.02°, and a two second dwell. The machine was operated at 40 kV and 35 mA using 2θ diffraction angles that varied between 10° and 100°. The JCPDS-ICDD powder diffraction database was used to characterise films.

2.5 Scratch testing

Scratch testing was carried out on coatings deposited onto an M42 high speed steel substrate using a Teer Coatings ST3001 scratch tester with a Rockwell Diamond indenter tip of radius 0.2 mm. A linear scratch velocity of 10 mm min^{-1} was employed, with the normal load being increased from 10 N to 100 N at a rate of 100 N min^{-1}. The system used can determine failure load to a precision of 0.03%. Tests were terminated if either a frictional force of 30 N was reached or total failure of the coating occurred. Single measurements were made.

2.6 Corrosion testing

Salt-spray testing of the coated substrates was carried out in accord with ASTM B117. The coated 440C SS discs were quartered, and the backs and sides of the quarter samples were masked with lacquer (from MacDermid) to ensure that only the coated surface (around 240 mm^2) was exposed; two separate samples were examined in the salt-spray test for each coating type and surface / process condition.

During the salt-spray test, samples were inspected every 15 minutes for the first four hours of exposure, and every hour thereafter. At each inspection, the samples were removed from the chamber, washed of any excess salt or corrosion product and dried before being photographed.

Image analysis of the photographs of the exposed samples was carried out, using ImageJ software (National Institutes of Health, Bethesda, Maryland, USA), to determine the percentage coverage of the exposed surfaces with corrosion products. Repeat tests were conducted for each coating type. Further corrosion tests were carried out using potentiodynamic testing. Samples were cut to 10 x 10 mm and mounted in Dap Mount Blue hot mounting resin from MetPrep Ltd. Using a 2.5 mm drill followed by M3 tap, a hole was created in the back of the mount reaching the back of the sample. The sample was then cleaned and a copper rod was inserted into the back until it made connection with the back of the sample, the connection was tested using a voltmeter. Following this the copper rod and sample were coated in lacquer, coating only the edges of the sample face, leaving as much of the face exposed as possible. The exposed area was then measured for use in calculating current density.

Tests were carried out using a VoltaLab PGZ 100 Potentiostat and Voltamaster 4 software. A platinum auxiliary electrode was used and a saturated potassium chloride electrode was used as a reference. The test was carried out in 5 wt% salt solution made by dissolving 52.6 g of NaCl in 1000 g of de-ionised water. All equipment was cleaned and rinsed in deionised water before testing. The system was deoxygenated by pumping nitrogen for 1 hour. After an hour the nitrogen was turned off, the temperature of the solution was measured and an open circuit potential scan was run. A potential linear voltage scan was then run between -250 mV below OCP and 1500 mV at a scan rate of 0.5 mV s^{-1} and a sampling rate of 1 measurement per second. Two tests were conducted for each coating type.

The corrosion current (I_{corr}) was calculated using the Tafel method according to the 1st Stern equation [32]. Calculations of i_{corr} were carried out using Voltamaster 4 software. The parameters of smoothing, calculation zone and segment were varied until a line of best fit was reached. Corrosion potential (E_{corr}) and polarisation resistance (R_P) were measured by plotting potential Vs current density and drawing a line of best fit. E_{corr} was calculated at the point of

zero current density (i=0) and the polarisation resistance was measured by the gradient of the line $\left(\frac{\Delta E}{\Delta i}\right)$.

3 Results & discussion

3.1 Effect of multilayering

Cross sections of the multilayer Inconel 625/Cr coatings can be seen in Fig. 1. The layers in in the b_p100 nm and the b_p600 nm multilayer coatings (Fig. 1 a & b) are clearly visible, however the individual layers in the b_p20 nm multilayer coating (Fig. 1c) cannot be clearly seen due to the resolution of the SEM.

X-ray diffraction patterns from the monolithic Inconel 625 and multilayer Inconel 625/Cr coatings are presented in Fig. 2. In addition the expected peak positions for Cr and Inconel 625 are indicated using JCPDS card numbers 6-0694 and 33-0397 respectively. Peaks corresponding to Cr can be seen for each multilayer coating. In each case the strongest peak was for the {1 1 0} planes at 44.4^o 2θ, Cr peaks were also observed for the {2 0 0}, {2 1 1} and {2 2 0} planes at 64.6^o, 81.7^o and 98.1^o 2θ respectively. Inconel 625 peaks are seen for each coating, the strongest being for the {1 1 1} planes at 43.4^o 2θ, however this is not distinct for the b_p20 nm coating. A small peak at 74.3^o 2θ, corresponding to the Inconel 625 {220} planes is present in the spectra from all coatings. The presence of crystalline Cr and Inconel 625 in each multilayered coating was therefore confirmed. Comparisons of the spectra with the expected peak height ratios from the reference cards indicates that there is preferential diffraction from the {1 1 0} Cr planes and from the {1 1 1} Inconel 625 planes, indicating that these are preferential growth directions. Peak broadening was observed for the multilayered coatings, as expected, the thinner the bilayer period the greater the broadening.

Fig. 3 shows results of the scratch tests for multilayer coatings alongside that of a monolithic Inconel 625 coating. All multilayer coatings outperformed the monolithic Inconel 625 coating

which failed at 33 N. There is a clear trend in behaviour, with the thinner bilayer period multilayer Inconel 625/Cr coatings requiring higher scratch loads for total film failure; the multilayer Inconel 625/Cr coating with b_p 20 nm exhibited the highest loads for film failure in the scratch tests, with total failure being observed under a load of 92 N. This enhancement of scratch resistance as a result of multilayering is expected, having been previously reported elsewhere [33, 34].

Results from salt spray tests are shown in figure 4. Comparison of the results for the monolithic Inconel 625 coating and the multilayer Inconel 625/Cr coatings reveals that corrosion resistance was not improved by the use of multilayers. There is no clear correlation between the barrier performance and multilayer repeat thickness, i.e. there was no correlation between corrosion performance and the number of layer interfaces per unit thickness of the coating. Fig. 5a shows a cross-section through an area of a b_p100 nm sample after 18 h of salt spray testing. Corrosion products can be seen both above and below the coating. It is clear that extensive substrate corrosion has occurred, the coating itself is cracked but there are no signs of extensive corrosion. This image clearly demonstrates that the poor corrosion resistance was not due to corrosion of the coating itself, but was associated with the inability of the coating to form an effective barrier to the corrosive media reaching the substrate. As seen in the SEM image in Fig. 5b, as corrosion of the substrate proceeds, corrosion products expanding and pushing up from below the coating can result in coating delamination and a large increase in the apparent area of corrosion, even though the coating material itself does not appear to be corroding. The coating has clearly not acted as an effective barrier between the substrate and the corrosive media.

Cross-sectional SEM imaging of the coated substrates has allowed various different types of defects to be identified. Fig. 6a shows a defect that penetrates all the way through the coating that is clearly related to a macroscopic surface feature. This also illustrates how the PVD coating

morphology closely follows that of the underlying surface. In Fig. 6b, cone defects can be observed; it has been previously reported that these result from contaminant particles which are either already present on the substrate surface or which are generated by the sputtering source and land on the surface during deposition [8, 12]. In Fig.6c the contrasting multilayers make it easy to see how defects initiating on the surface result in disruption that propagates the thickness of the coating. Fig. 6d shows a location where corrosion of the substrate has occurred underneath a region of the coating containing defects, again the disruption to the multilayers makes the location of the defects easily visible. The inability of the coating to act as an effective barrier between the substrate and the corrosive media is attributed to the presence of defects in the coatings which provide effective paths for the corrosive media to reach the substrate.

3.2 Effect of substrate surface and deposition conditions on corrosion behaviour

The results of salt-spray tests carried out on coatings deposited under different deposition conditions and with different surface preparations are shown in Fig. 7. Results from two samples of each type are included as well as a sample of the uncoated 440C SS substrate. The majority of the coated samples perform better than the uncoated 440C SS. The samples with different initial surface preparations can be ranked in the following order of increasing corrosion resistance: 1200 grit, workshop grind and polished surface. The polished surface finish substrate exhibited a significantly lower corrosion rate compared to the rest of the coatings, with one sample showing no corrosion for the first eight hours. There is no significant difference between the 1200 grit surface samples and the uncoated 440C SS.

The effect of deposition process was determined using 1200 grit surface samples. The intermediate etch process does improve corrosion resistance. Of the interrupted process samples, one performs better than the standard process 1200 grit samples and one worse. All other sample types have a reasonable sample to sample reproducibility.

Potentiodynamic testing was carried out to further explore the corrosion behaviour of coatings deposited on different substrate surface finishes and under different deposition conditions. The results are shown in Figs. 8 & 9 and Table 3 respectively.

For coatings deposited on different surface roughness substrates (Fig. 8), all coatings exhibited a larger sample to sample variation than was seen for the uncoated 440C SS substrate. The corrosion potential of the coated samples is either more positive than that of the uncoated 440C SS substrate or approximately the same as the 440C SS substrate. The anodic sections of the potentiodynamic results show that the PVD coatings do decrease the corrosion current density. The only exception to this is the initial anodic region of the initial 1200 grit sample, which has a corrosion potential similar to that of the uncoated 440C SS. No evidence of passivation is seen. The samples cannot be ranked in terms of corrosion resistance based on the potentiodynamic results as the scatter due sample to sample variation and the coating type to coating type variation overlap.

For coatings deposited under different deposition conditions (Fig. 9), it can again be seen that the PVD coatings decrease the corrosion current density, i.e. improve corrosion resistance. The only exception to this is again the initial anodic region of the initial 1200 grit sample, which has a corrosion potential similar to that of the uncoated 440C SS. Sample to sample variation in both corrosion current density and corrosion potential are again seen to be of a similar magnitude to the variation due to coating type. Some indication of passivation is seen in the results for samples with the intermediate etch as well as for the samples generated by the interuppted process.

3.3 Effect of substrate surface and deposition conditions on defect populations

Fig. 10 shows SEM images of the surface topography of the various versions of the multilayer Inconel 625/Cr (b_p100 nm) coatings. Comparison of Figs. 10a-c clearly shows that the substrate surface finish does affect the defect type and distribution in the deposited coatings. The coating

deposited on the workshop ground sample (Fig. 10a) has a large number of both linear and nonlinear growth defects. That on the 1200 grit surface has linear features but few large nonlinear growth defects (Fig. 10b) and the coating on the 6 µm polished substrate appears largely featureless (Fig. 10c). Reducing the substrate surface roughness appeared to reduce the defect density of all types of defects. Comparison of Figs 10 b,d&e shows that effect of the different coating deposition processes is less distinct than the effect of the substrate roughness.

Fig. 11 shows examples from each of the defect categories used to generate Fig. 12. Fig. 12 shows defect density results, a clear reduction in defect density with decreasing substrate surface roughness is seen: coatings deposited on a 1200 grit substrate surface finish (Ra = 78 nm) showed a lower defect density than those deposited on a rougher, workshop grind substrate, (Ra = 126 nm) and coatings deposited on the polished substrate (Ra = 12 nm) showed the lowest defect density. The population of each defect type decreases with decreasing surface roughness.

Coatings deposited under interrupted and intermediate etch conditions, both showed higher defect densities than coatings deposited on the 1200 grit surface finish substrate under non-interrupted conditions. The coating deposited under intermediate etch conditions exhibited the highest number of defects out of all conditions.

4 Discussion

The cross sections shown in Fig.5 confirm that, for the multilayer Inconel 625/Cr coatings used in this work, corrosion of the system is not due to corrosion of the coatings themselves but by the ineffectiveness of the coatings as a barrier between the corrosive media and the substrate material. The salt spray results in Fig.4 show that multilayering itself does not improve the corrosion resistance of the coating, i.e. that the interfaces in the multilayered structure do not improve the barrier behaviour of the coatings. This indicates both that the corrosion behaviour is dominated by through thickness defects which breach the coating and that, as Fig. 6

illustrates, multilayering does not block these defects. The addition of more significant disruption to the deposition process by the use of a. process interruption and b. an intermediate etch, did not decrease, or significantly change, the surface defect densities.

The XRD results indicate that both the Inconel 625 and Cr have preferential growth directions, the high relative intensity of both the Cr{1 1 0} and Inconel 625{1 1 1} planes indicates that the preferential growth of each crystal system has resulted in alignment of these planes, i.e. alignment of the body centred cubic Cr{1 1 0} and face centred cubic Inconel 625{1 1 1} planes. This is the well known Kurdjumov-Sachs orientational relationship (KSOR) [35]. The good fit between the Inconel 625 and Cr crystal structures that the KSOR produces means that the Inconel 625/Cr interfaces are semi-coherent. The structural disruption associated with the interface is therefore minimal, meaning that any lattice disruption caused by defects can easily continue across the interface instead of being blocked.

Fig. 12 shows that the substrate surface roughness clearly influences the resultant defect density, with populations of all defect types decreasing as surface roughness decreases. The improved salt spray corrosion resistance of the polished samples is attributed to the decreased defect density. However, it is not possible from these results to determine which, if any, specific defect type is most important.

It must be noted that the corrosion results show significant variations for corrosion current density, corrosion potential and polarisation resistance for nominally identical samples. This is consistent with corrosion being due to defects that are randomly distributed across the sample.

It is clear that neither of the two modified deposition processes decrease the population of defects. Comparison of the defect populations with that for the coating produced with the standard process on the 1200 grit substrate show that both modified processes increase the total number of defects (Fig. 12). This is largely due to the increase in the population of circular defects. This could be attributed to dust or particles (which remain in the chamber even after

cleaning) being moved during the pumping stage and landing on the sample surface. This process happens twice for the modified deposition processes and only once for the standard process, hence an increase in the population of any associated defects would be expected.

5 Conclusions

The results and analysis presented in this paper show that for the Inconel 625/Cr system considered, the following conclusions can be drawn:

- Multilayering in this system does not improve corrosion-barrier performance.
- Corrosion behaviour is determined by the presence of defects which provide pathways for corrosive media through the coatings.
- Neither multilayering nor process interruption block these defects for the Inconel 625/Cr system used in this work, this is due to the KSOR.
- The surface finish of the substrate affects the defect type and density within the PVD coating and can have a significant effect on the salt-spray corrosion-barrier performance.
- The corrosion barrier performance of the b_p100 nm multilayer Inconel 625/Cr coating was significantly increased for coatings deposited on a polished substrate.
- The somewhat random nature of the spatial distribution of defects introduces variation into the corrosion results.

Acknowledgements

We acknowledge Teer Coatings Ltd, Miba Coatings Group for their work on the coatings and Rolls-Royce plc for funding this work.

References

1. **Regulation (EC) No 1907/2006,** ***Concerning the Registration, Evaluation, Authorisation and Restriction of Chemicals (REACH), establishing a European Chemicals Agency, amending***

Directive 1999/45/EC and repealing Council Regulation (EEC) No 793/93 and Commission Regulation (EC) No 1488/94 as well as Council Directive 76/769/EEC and Commission Directives 91/155/EEC, 93/67/EEC, 93/105/EC and 2000/21/EC. 2007. p. L136/3.

2. Sree Harsha, K.S., *Principles of Physical Vapor Deposition of Thin Films*. 2006, Oxford: Elsevier. p. 961.
3. Ohring, M., *The Materials Science of Thin Films*. 1992, San Diego: Academic Press. p. 133 – 141
4. Shaha, K.P., Y.T. Pei, C.Q. Chen, and J.T.M. De Hosson, *Synthesis of ultra-smooth and ultra-low friction DLC based nanocomposite films on rough substrates.* Thin Solid Films, 2010. 519(5): p. 1618-1622.
5. Lewis, D.B., S.J. Creasey, C. Wüstefeld, A.P. Ehiasarian, and P.E. Hovsepian, *The role of the growth defects on the corrosion resistance of CrN/NbN superlattice coatings deposited at low temperatures.* Thin Solid Films, 2006. 503(1–2): p. 143-148.
6. Lee, S.-C., W.-Y. Ho, and F.D. Lai, *Effect of substrate surface roughness on the characteristics of CrN hard film.* Materials Chemistry and Physics, 1996. 43(3): p. 266-273.
7. Brandl, W. and C. Gendig, *Corrosion behaviour of hybrid coatings.* Thin Solid Films, 1996. 290–291: p. 343-347.
8. Panjan, P., M. Čekada, M. Panjan, and D. Kek-Merl, *Growth defects in PVD hard coatings.* Vacuum, 2009. 84(1): p. 209-214.
9. Čekada, M., P. Panjan, D. Kek-Merl, M. Panjan, and G. Kapun, *SEM study of defects in PVD hard coatings.* Vacuum, 2007. 82(2): p. 252-256.
10. Panjan, P., M. Čekada, M. Panjan, D. Kek-Merl, F. Zupanič, L. Čurković, and S. Paskvale, *Surface density of growth defects in different PVD hard coatings prepared by sputtering.* Vacuum, 2012. 86(6): p. 794-798.
11. Ries, L.A.S., D.S. Azambuja, and I.J.R. Baumvol, *Corrosion resistance of steel coated with Ti/TiN multilayers.* Surface and Coatings Technology, 1997. 89(1–2): p. 114-120.
12. Panjan, P., D. Kek Merl, F. Zupanič, M. Čekada, and M. Panjan, *SEM study of defects in PVD hard coatings using focused ion beam milling.* Surface and Coatings Technology, 2008. 202(11): p. 2302-2305.
13. Carvalho, N.J.M. and J.T.M. DeHosson, *Microstructure investigation of magnetron sputtered WC/C coatings deposited on steel substrates.* Thin Solid Films, 2001. 388(1–2): p. 150-159.
14. Durst, O., J. Ellermeier, and C. Berger, *Influence of plasma-nitriding and surface roughness on the wear and corrosion resistance of thin films (PVD/PECVD).* Surface and Coatings Technology, 2008. 203(5–7): p. 848-854.
15. Svahn, F., Å. Kassman-Rudolphi, and E. Wallén, *The influence of surface roughness on friction and wear of machine element coatings.* Wear, 2003. 254(11): p. 1092-1098.
16. Maeng, S., L. Axe, T. Tyson, L. Gladczuk, and M. Sosnowski, *Corrosion Behavior of Magnetron Sputtered Alpha Ta Coatings on Smooth and Rough Steel Substrates.* Surface & Coatings Technology, 2006. 200: p. 5717 - 5724.
17. Liu, C., A. Leyland, S. Lyon, and A. Matthews, *An a.c. impedance study on PVD CrN-coated mild steel with different surface roughnesses.* Surface and Coatings Technology, 1995. 76–77, Part 2: p. 623-631.
18. Panjan, P., P. Gselman, D. Kek-Merl, M. Cekada, M. Panjan, G. Drazic, T. Boncina, and F. Zupanič, *Growth defect density in PVD hard coatings prepared by different deposition techniques.* Surface & Coatings Technology, 2013. 237: p. 349–356.
19. Fenker, M., M. Balzer, H.A. Jehn, H. Kappl, J.J. Lee, K.H. Lee, and H.S. Park, *Improvement of the corrosion resistance of hard wear resistant coatings by intermediate plasma etching or multilayered structure.* Surface and Coatings Technology, 2002. 150(1): p. 101-106.
20. Liu, C., Q. Bi, H. Ziegele, A. Leyland, and A. Matthews, *Structure and corrosion properties of PVD Cr-N coatings.* Journal of Vacuum Science & Technology A: Vacuum, Surfaces, and Films, 2002. 20(3): p. 772-780.
21. Jehn, H.A., *Improvement of the corrosion resistance of PVD hard coating–substrate systems.* Surface and Coatings Technology, 2000. 125(1–3): p. 212-217.

22. **Mori, T., S. Fukuda, and Y. Takemura, *Improvement of mechanical properties of Ti/TiN multilayer film deposited by sputtering.* Surface and Coatings Technology, 2001. 140(2): p. 122-127.**
23. **Park, H.S., H. Kappl, K.H. Lee, J.J. Lee, H.A. Jehn, and M. Fenker, *Structure modification of magnetron-sputtered CrN coatings by intermediate plasma etching steps.* Surface and Coatings Technology, 2000. 133–134: p. 176-180.**
24. **Fenker, M., M. Balzer, and H. Kappl, *Corrosion behaviour of decorative and wear resistant coatings on steel deposited by reactive magnetron sputtering – Tests and improvements.* Thin Solid Films, 2006. 515(1): p. 27-32.**
25. **Bayón, R., A. Igartua, X. Fernández, R. Martínez, R.J. Rodríguez, J.A. García, A. de Frutos, M.A. Arenas, and J. de Damborenea, *Corrosion-wear behaviour of PVD Cr/CrN multilayer coatings for gear applications.* Tribology International, 2009. 42(4): p. 591-599.**
26. **Bobzin, K., N. Bagcivan, S. Theiß, R. Weiß, U. Depner, T. Troßmann, J. Ellermeier, and M. Oechsner, *Behavior of DLC coated low-alloy steel under tribological and corrosive load: Effect of top layer and interlayer variation.* Surface and Coatings Technology, 2013. 215: p. 110-118.**
27. **Dobrzański, L.A., K. Lukaszkowicz, J. Mikula, and D. Pakula, *Structure and corrosion resistance of gradient and multilayer coatings.* Journal of Achievements in Materials and Manufacturing Engineering, 2006. 18(1-2): p. 75-78.**
28. **Mellor, B.G., *Surface Coatings for Protection Against Wear*. 2006, Cambridge: Woodhead Publishing.**
29. **Matthews, A., *Plasma-based physical vapor deposition surface engineering processes.* Journal of Vacuum Science & Technology A: Vacuum, Surfaces, and Films, 2003. 21(5): p. S224-S231.**
30. **PalDey, S. and S.C. Deevi, *Single layer and multilayer wear resistant coatings of (Ti,Al)N: a review.* Materials Science and Engineering: A, 2003. 342(1–2): p. 58-79.**
31. **H. L. Eiselstein, D.J.T., *The Invention and Definition of Alloy 625.* The Minerals, Metals & Materials Society, 1991: p. 2.**
32. **Stern, M. and A.L. Geary, *Electrochemical Polarization: I . A Theoretical Analysis of the Shape of Polarization Curves.* Journal of The Electrochemical Society, 1957. 104(1): p. 56-63.**
33. **Cabrera, G., J.C. Caicedo, C. Amaya, L. Yate, J. Muñoz Saldaña, and P. Prieto, *Enhancement of mechanical and tribological properties in AISI D3 steel substrates by using a non-isostructural CrN/AlN multilayer coating.* Materials Chemistry and Physics, 2011. 125(3): p. 576-586.**
34. **Araujo, J.A., G.M. Araujo, R.M. Souza, and A.P. Tschiptschin, *Effect of periodicity on hardness and scratch resistance of CrN/NbN nanoscale multilayer coating deposited by cathodic arc technique.* Wear, 2015. 330–331: p. 469-477.**
35. **Kurdjumov, G. and G. Sachs, *Über den Mechanismus der Stahlhärtung.* Zeitschrift für Physik, 1930. 64(5): p. 325-343.**

Tables

Table 1. Chemical composition(wt %) of M42 high speed steel and 440C stainless steel (SS) substrates as determined by optical emission spectroscopy.

Element	440C	M42
Fe	80.0 ± 0.20	80.2 ± 0.80
C	1.06 ± 0.01	0.82 ± 0.02
Si	0.45 ± .0.25	0.32 ± 0.02
Mn	0.33 ± 0.01	0.33 ± 0.01
P	0.02 ± 0.01	<0.03
S	0.01 ± 0.01	<0.02
Cr	17.10 ± 0.10	5.10 ± 0.57
Mo	0.44 ± 0.00	4.58 ± 0.19
Ni	0.20 ± 0.01	0.49 ± 0.33
Al	0.03 ± 0.08	<0.03
Co	0.02 ± 0.00	<0.08
Cu	0.04 ± 0.01	<0.10
Nb	0.01 ± 0.01	0.04 ± 0.02
Ti	<0.01	<0.01
V	0.09 ± 0.01	1.85 ± 0.01
W	<0.03	6.06 ± 0.11
Pb	<0.05	<0.05

Table 2. Typical composition(%) of Inconel 625 [27].

Ni	Cr	Mo	Nb	Fe	C	Si	Al	Ti	Mn	S
61	21.5	9	3.6	2	0.05	0.20	0.20	0.20	0.20	0.001

Table 3. Polarisation resistance (R_P), i_{corr} and E_{corr} values from potentiodynamic tests on multilayer Inconel 625/Cr coatings (b_p100 nm) deposited on different surface finishes and under different deposition conditions, in 5 wt% NaCl solution

	Initial tests			Repeat tests		
Sample	**R_P (ohm.cm²)**	**i_{corr} (µA/cm²)**	**E_{corr} (V)**	**R_P (ohm.cm²)**	**i_{corr} (µA/cm²)**	**E_{corr} (V)**
SS	26728	0.580	-0.411	25907	0.212	-0.445
Coated SS (WG)	48704	0.397	-0.259	-	-	-
Coated SS (1200)	23617	0.654	-0.469	24176	0.421	-0.264
Coated SS (Polish)	21950	0.318	-0.442	29821	0.163	-0.346
Coated SS (interrupted)	38315	0.186	-0.393	42223	0.197	-0.417
Coated SS (etch)	40218	0.114	-0.386	28933	0.339	-0.422

Figures

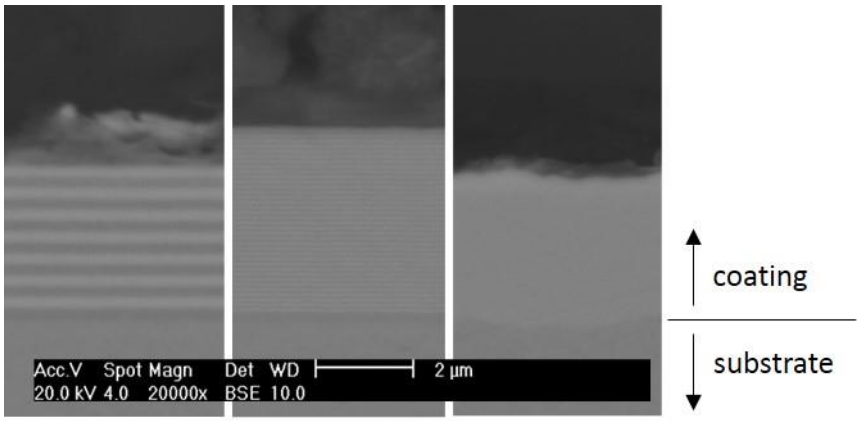

Figure 1 cross sectional SEM images of multilayer Inconel 625/Cr coatings. (a) b_p600 nm layers, (b) b_p100 nm layers and (c) b_p20 nm layers

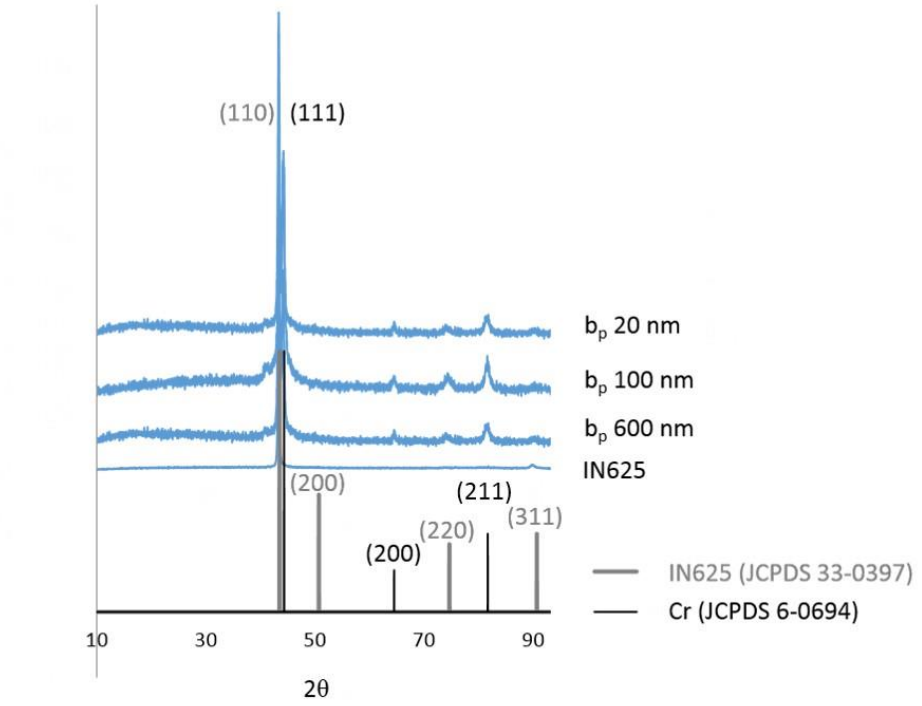

Figure 2 XRD patterns of Inconel 625, multilayer Inconel 625/Cr (b_p600 nm), multilayer Inconel 625/Cr (b_p100 nm) and multilayer Inconel 625/Cr (b_p20 nm) coatings on 440C SS substrates. Reference peaks for Inconel 625 and Cr are also shown.

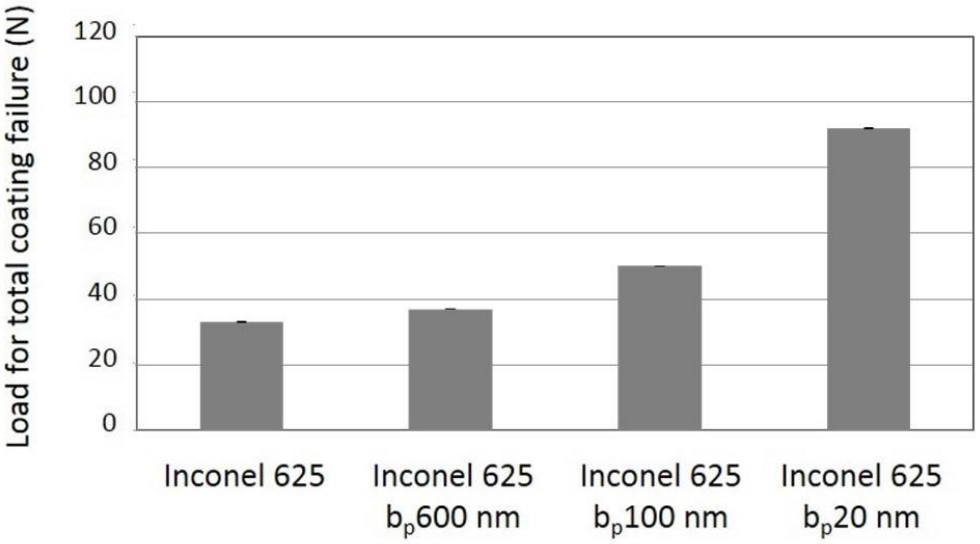

Figure 3 Load at total failure for each coating during scratch tests. Results presented are from single tests, the error bars indicate the 0.03% precision of the system.

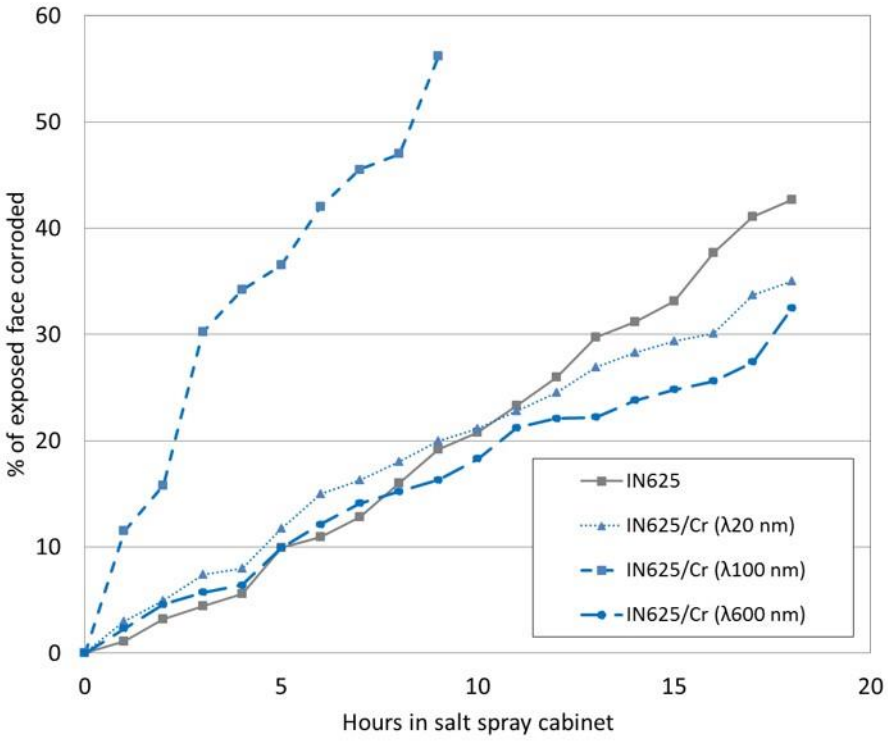

Figure 4 Salt spray results for monolithic Inconel 625 coating and multilayer coatings.

a 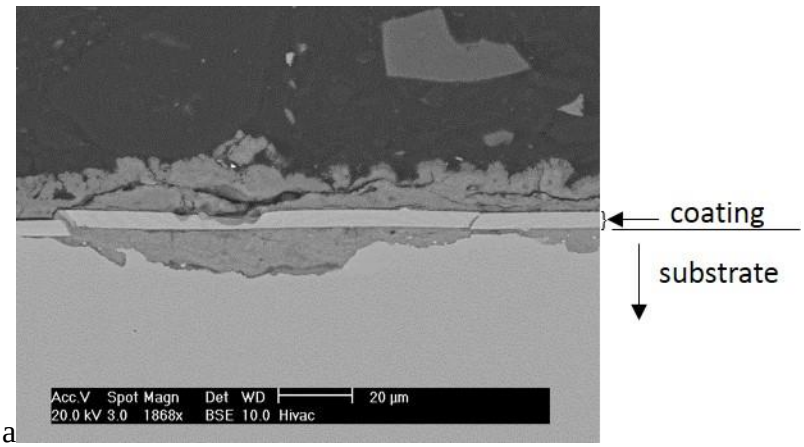

b 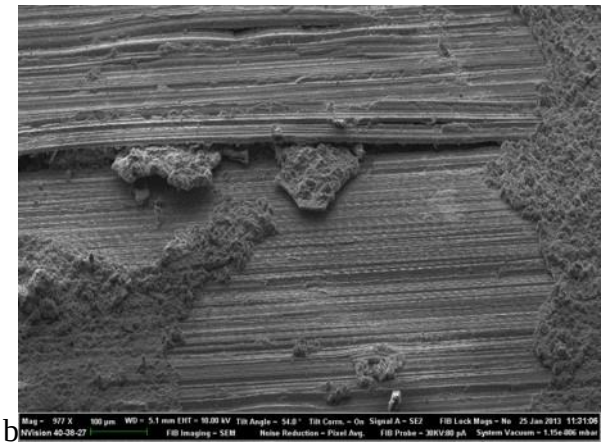

Figure 5. (a) Cross-sectional SEM image of multilayer Inconel 625/Cr coating (b_p100 nm) showing corrosion of the substrate and a broken coating, (b) Top surface SEM image of multilayer Inconel 625/Cr coating (b_p100 nm) with corrosion pushing up from beneath the coating causing coating delamination

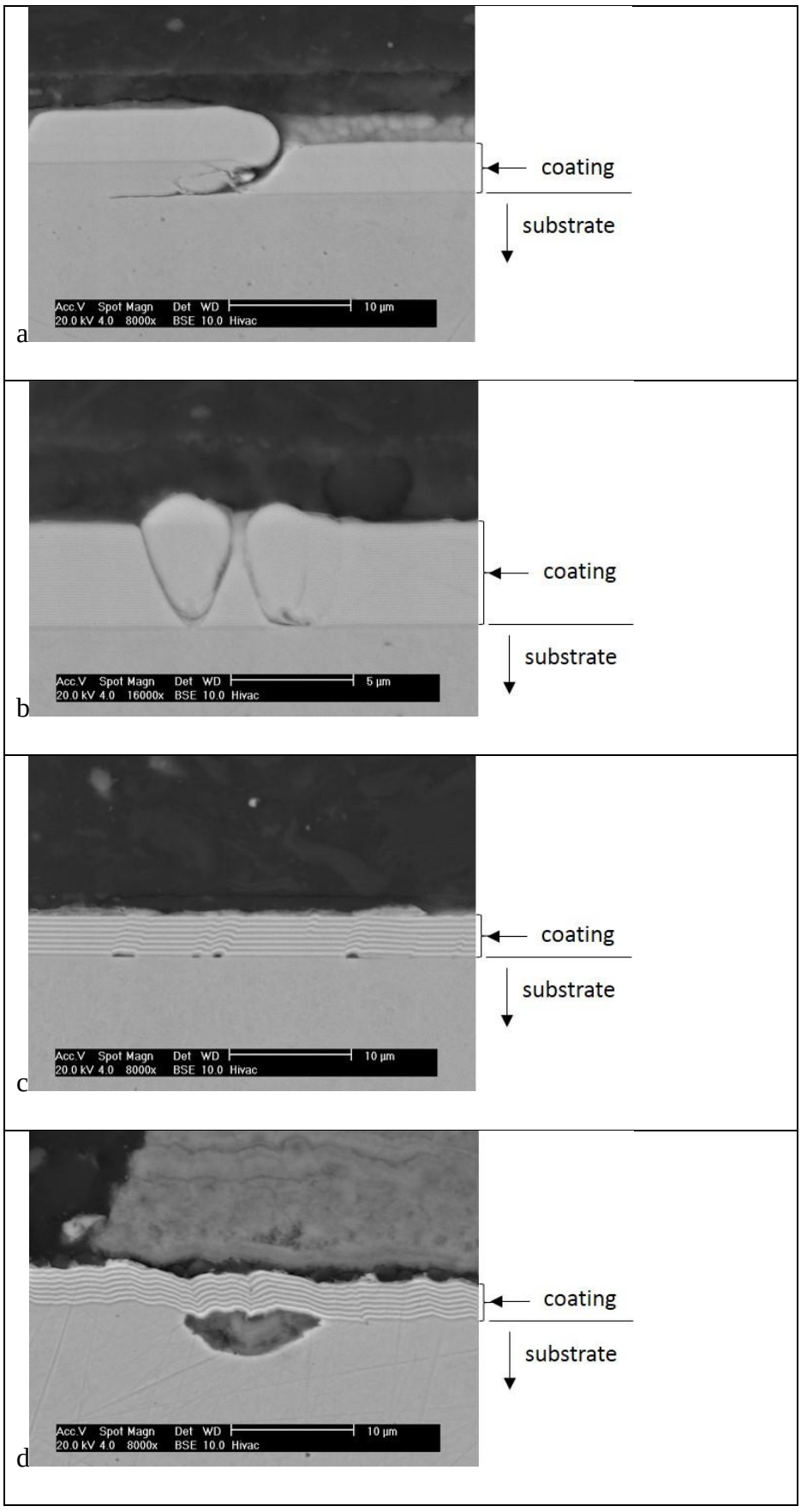

Figure 6 Cross sectional SEM images of growth defects (a) (b) (c) (d)

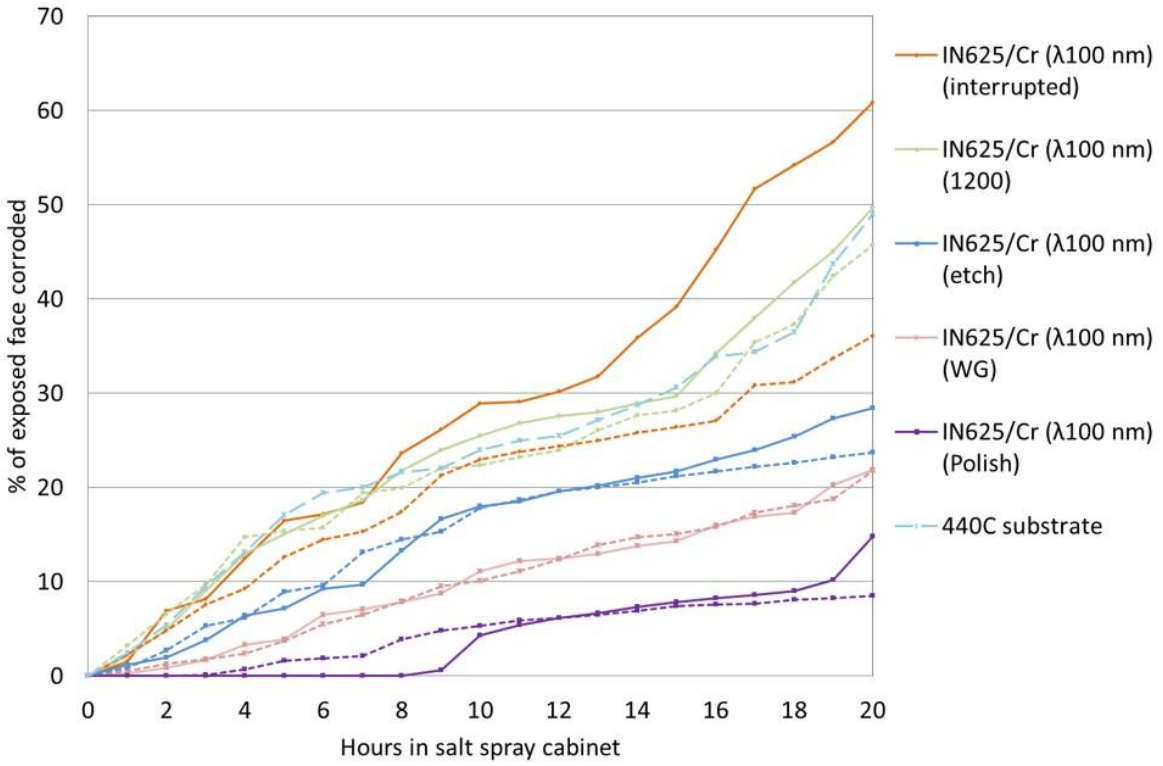

Figure 7 Salt spray results of multilayer Inconel 625/Cr coatings (b_p100 nm) on 440C SS substrates prepared on different substrate surface finishes and under different deposition conditions, *dotted lines shows repeat tests

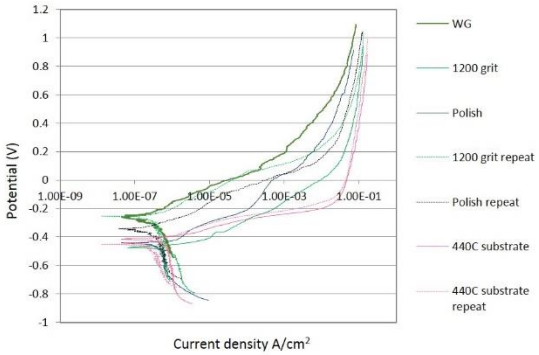

Figure 8 Potentiodynamic results for coatings deposited on different roughness substrates

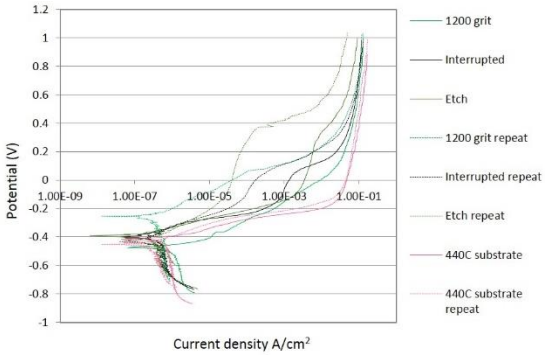

Figure 9 Potentiodynamic results for coatings deposited under different deposition conditions

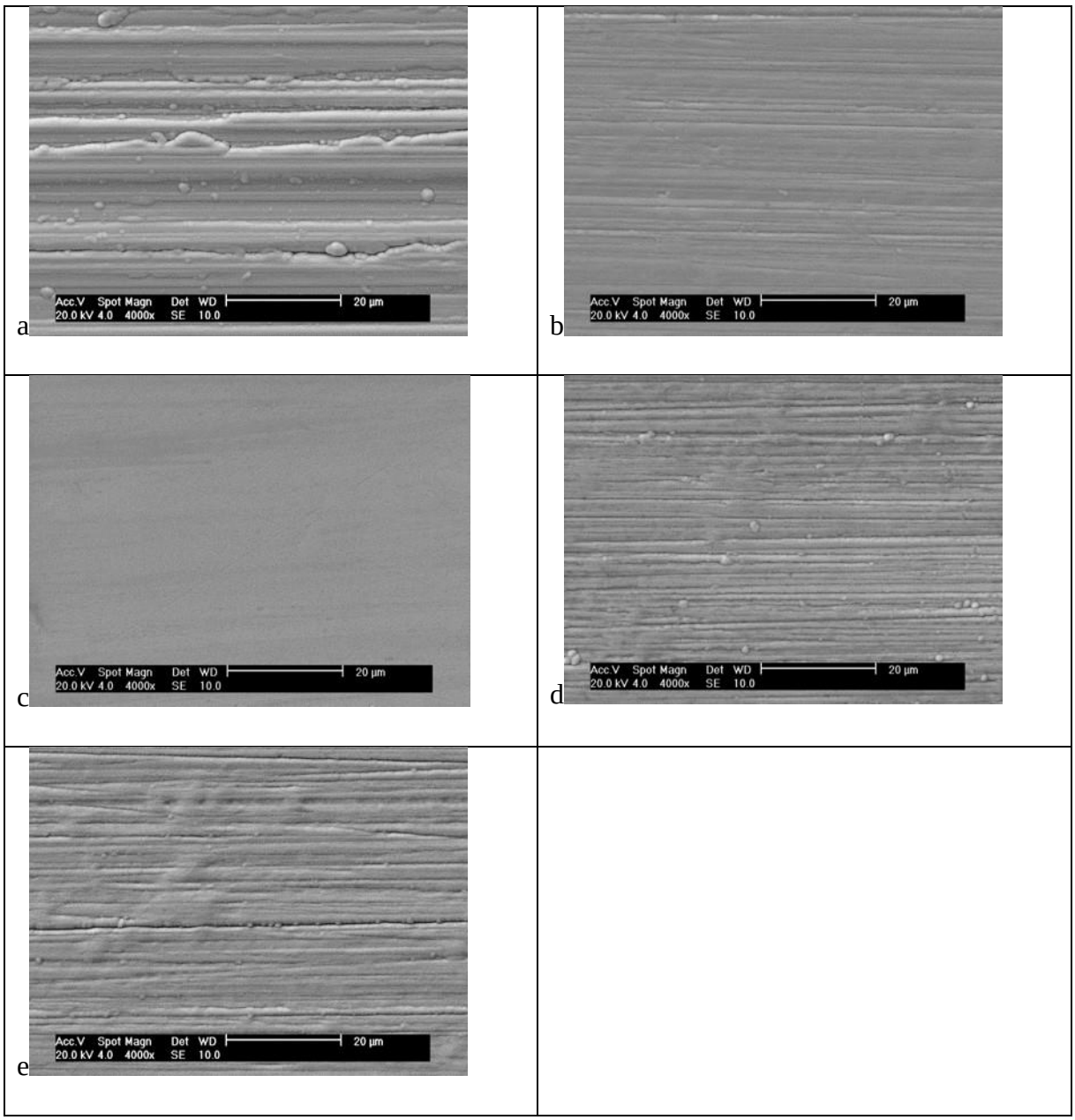

Figure 10 SEM images of the surface topography of the multilayer Inconel 625/Cr coatings (b_p100 nm) deposited on substrates using five different preparation techniques: (a) workshop grind, (b) 1200 grit grind, (c) 6 µm polish, (d) intermediate etch conditions and (e) interrupted conditions.

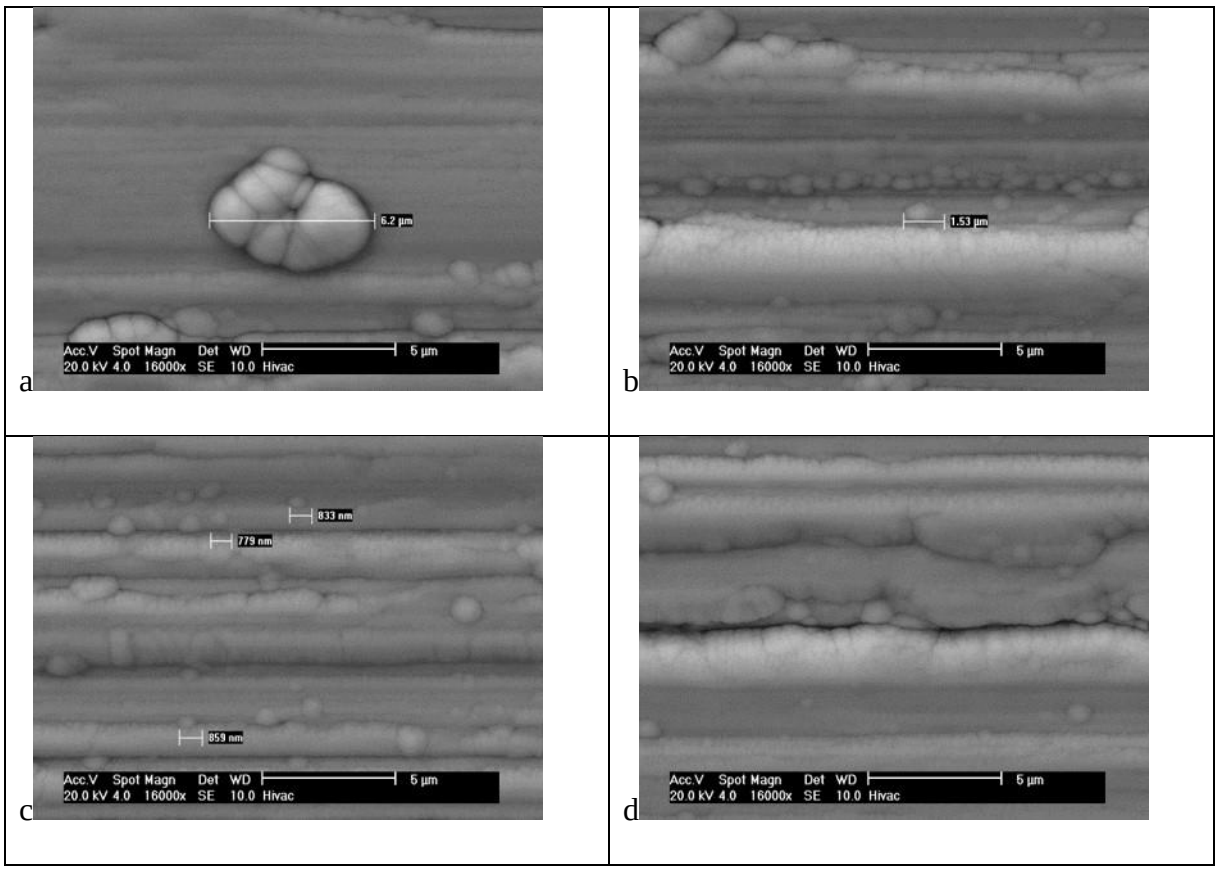

Figure 11 Categories of defects on multilayer Inconel 625/Cr coatings (b_p100 nm), deposited on different substrate surface roughnesses (a) a >3 µm defect on a WG substrate (b) a 1-3 µm defect on a WG substrate (c) <1 µm defects on a WG substrate (d) linear defects on a WG substrate

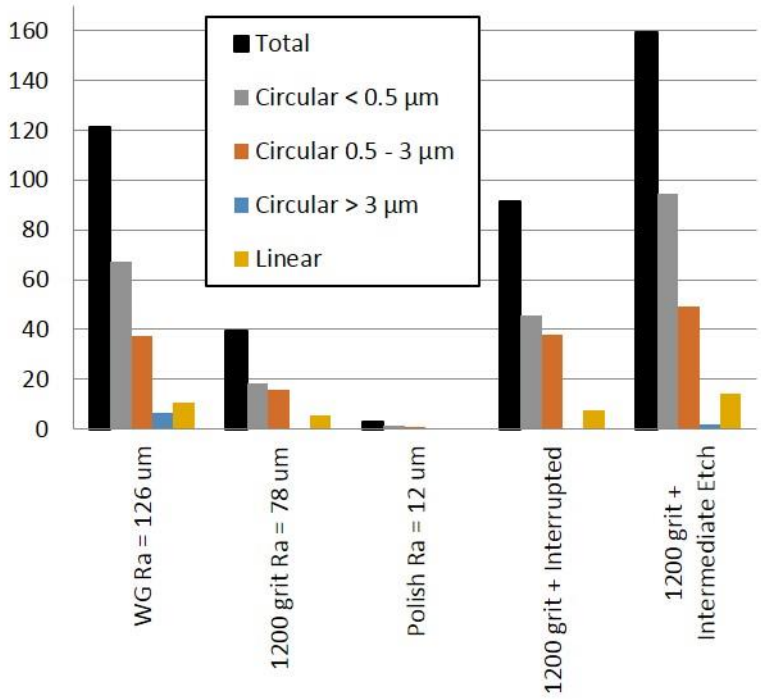

Figure 12 Number of defects in a 4300 µm^2 area on multilayer Inconel 625/Cr coatings (b_p100 nm), on different surface roughness substrates and under different deposition conditions.